ORIGINAL PAPER

S. Quartieri · M. C. Dalconi · F. Boscherini · R. Oberti
F. D'Acapito

Changes in the local coordination of trace rare-earth elements in garnets by high-energy XAFS: new data on dysprosium

Abstract The site location and local geometry of trace amounts (299 ppm) of dysprosium in a natural melanite garnet from a carbonatitic rock have been studied by high-energy fluorescence-detected X-ray absorption fine-structure spectroscopy (XAFS). Measurements were done at the Dy K-edge (53789 eV). Data analysis shows that Dy (i.r. = 0.98 Å) is incorporated at the X site, similarly to other REE, namely Nd (i.r. = 1.11 Å) and Ce (i.r. = 1.14 Å). Comparison of the XAFS data obtained for these three REE and for Ca shows that, within a given garnet composition, the difference in the local geometry can be modelled in terms of differences in the ionic radii. On the contrary, the local coordination of the individual cations is different in distinct garnet compositions, in contrast to what was suggested by previous atomistic simulations of the garnet structure. Comparison of the local coordination geometries available in the literature shows that the Young modulus of the X site strongly depends on the major-element composition of all the structural sites. Both these points are important for Earth Sciences, and especially for geochemical modelling of trace-element incorporation and partitioning.

S. Quartieri (✉)
Dipartimento di Scienze della Terra,
Salita Sperone 31, 98166 Messina S. Agata, Italy
e-mail: simonaq@unimo.it
Tel.: +39-090-6765096
Fax: +39-090-392333

M. C. Dalconi
Dipartimento di Scienze della Terra,
C.so Ercole I_0 d'Este 32, 44100 Ferrara, Italy

F. Boscherini
INFM and Dipartimento di Fisica, Università di Bologna,
Viale Berti Pichat 6/2, 40127 Bologna, Italy

R. Oberti
CNR, Istituto di Geoscienze e Georisorse,
sezione di Pavia, via Ferrata 1, 27100 Pavia, Italy

F. D'Acapito
INFM, Operative Group in Grenoble,
c/o European Synchrotron Radiation Facility,
GILDA CRG, BP 220, 38043 Grenoble, France

Introduction

The accurate knowledge of trace-element behaviour in rock-forming and accessory minerals is fundamental to understand and model petrologic and geochemical processes. This behaviour is generally investigated based on the observed trends of the measured mineral/melt partition coefficients ($^{S/L}D$). Partition coefficients of rather homogeneous series of isovalent cations (e.g. REE) are generally modelled based on the elastic-strain theory (Beattie 1994; Blundy and Wood 1994, 2003; Wood and Blundy 1997, 2002). In this framework, the different values of the partition coefficients are explained by the different strain induced in a perfectly elastic and isotropic crystal lattice upon the substitution of the major component at a given structural site by a trace element with different ionic radius. Near-parabolic trends are derived, which have a maximum (strain-free partition coefficient, D_0) at the effective ionic radius (r_0) of the site, and an amplitude (E) which is inversely related to the Young's modulus of the site. The results of this approach should, however, be validated on the basis of their congruity with the measured dimensions and bulk moduli of the relevant sites. These parameters are generally measured by techniques (such as the structure refinement) which provide an image averaged over the crystal investigated. Rock-forming minerals are always complex solid solutions; therefore, the only approach capable of characterising the local coordination of the individual substituents is the use of element-selective spectroscopic methods.

Garnets are a group of rock-forming minerals of great relevance for petrogenetic studies, since they are stable over a wide range of physicochemical conditions and are able to incorporate significant amounts of several trace elements commonly used in geochemical modelling. For these reasons, aluminosilicate garnets ($X_3Al_2Si_3O_{12}$, $X = Fe^{2+}$, Mn^{2+}, Mg, Ca) have received

much attention, regarding both their complex major-element crystal chemistry (Merli et al. 1995; Ungaretti et al. 1995), their thermodynamic properties (see for a review Geiger 1999, 2000; Geiger and Armbruster 1997), and their trace-element behaviour (Salters and Longhi 1999; Van Westrenen et al. 1999, 2000, 2001, 2003). In particular, Van Westrenen et al. (2001) found strong variations in both the r_0 and E calculated along the pyrope–grossular join (i.e. $Mg_3Al_2Si_3O_{12}$–$Ca_3Al_2Si_3O_{12}$).

From a long-range perspective, detailed crystal-chemical studies have shown that the configuration of the X site in pyrope is different from that in grossular, thus suggesting that the local coordination of a given element at the X site in the solid-solution terms strongly depends on the garnet composition. This feature was ascribed to the great number of edges shared between the different polyhedra (namely six between X and Y, four between X and other X polyhedra, two between X and Z), which propagate the effects of the solid solution also to those site whose composition remains unchanged (Ungaretti et al. 1995). A XANES study at the Ca K edge done by Quartieri et al. (1995) on a series of natural samples in the (pyr,alm)–gro join supported the idea that the local coordination of Ca is different along the join.

In the short-range perspective, atomistic computer simulations of major and trace-element behaviour in the pyrope–grossular solid solution confirmed the strong geometrical and energetic differences between X sites occupied by Mg and by Ca, and stressed the role of third-nearest-neighbour interactions on trace-element solution energies and trace-element incorporation (Bosenick et al. 2000; Van Westrenen et al. 2003). However, Van Westrenen et al. (2003) concluded that the local geometry of a given element occurring at the X site is rather invariant along the solid solution. There is thus a need for direct information on the local coordination of the various cations substituting at the X site in various alumino-silicate garnet solid solutions. Because the bulk composition strongly affects site geometry, this information cannot simply be derived from the available structure refinements of some REE end-member garnets done by Euler and Bruce (1965).

X-ray absorption spectroscopy (Lee et al. 1981; Koninsberger and Prins 1988) is able to determine the local structural environment of most elements in the periodic table (cf. for a review: Calas et al. 1990; Quartieri 2003). In particular, when used in the fluorescence mode (XAFS), the technique acquires sensitivity to highly diluted elements, and thus becomes a powerful tool for the determination of local atomic environment around selected minor and trace elements in minerals. Previous applications of XAFS in garnets concerned the investigation of the location and site geometry of Yb (at the 1 wt% level) in synthetic pyrope and grossular (Quartieri et al. 1999a,b). Measurements were done at the L-edge, and data treatment showed that Yb is incorporated into the dodecahedral X site, and that its local geometry is different in pyrope than in

grossular, and also different from that of the proper major cation. The site preference and geometry of two trace LREE (Nd, ranging in concentration from 176 to 1074 ppm, and Ce in 791 ppm) in a melanite garnet has also been investigated by high-energy fluorescence XAFS spectroscopy. Both these elements were found to be incorporated into the dodecahedral X site, the difference in the local geometry being compatible with the ionic radii (Quartieri et al. 2002). Notably, these studies also discarded incorporation into defects or interstitial sites, which also would have affected models of partitioning as well as of diffusion rates.

Here we present the results obtained for a smaller REE, Dy, which is present with a concentration of 299 ppm (measured by ion microprobe) in one of the garnet specimens studied by Quartieri et al. (2002). Dy has an ionic radius (1.03 Å; Shannon 1976) significantly different from that of Ca (1.12 Å) and intermediate between those of Nd and Ce (1.11 and 1.14 Å) and that of Yb (0.985 Å). Comparison of the local geometry of L- and HREE in the same garnet specimen should provide a better understanding of the structural constraints on trace-element incorporation in garnet.

This work is also of interest from a methodological point of view, due to the extremely high energy (about 54 keV) of the Dy K-edge. The successful result of the experiment shows that, despite the high spectral broadening due to the short core-hole lifetime, analysable data can be obtained (at least in the EXAFS region). It also shows that third-generation synchrotron radiation X-ray sources and beamlines can provide sufficient flux to perform an experiment on an element with a concentration around 300 ppm.

Experimental methods and data analysis

The sample studied (A204) is a melanite garnet (i.e. Ti-rich ugrandite) occurring in an alkaline pegmatite from Afrikanda (Kola-Karelia; Russia). It has been characterised by electron microprobe (for major elements), by ion microprobe (for trace elements) and by single-crystal structure refinement. Details of the complete crystal-chemical characterisation of this garnet are reported in Quartieri et al. (2002, Tables 1–4). The resulting unit formula, calculated on the basis of 12 oxygen atoms, is: Si = 2.337, Ti = 0.889, Al = 0.280, Fe^{2+} = 0.137, Fe^{3+} = 1.199, Mn = 0.019, Mg = 0.146, Ca = 2.912, Na = 0.025, Zr = 0.039 atoms per formula unit (apfu); Sc = 62, Cr < 6, Sr = 114, Y = 1187, La = 133, Ce = 755, Nd = 1029, Sm = 357, Eu = 137, Gd = 345, Dy = 299, Er = 132, Yb = 109 ppm. In terms of site preference, the available data suggest that Fe^{3+} is partitioned between the tetrahedral and octahedral sites, whereas Ti, Zr, Al, Fe^{2+} and most Mg^{2+} occur at the octahedral site. Therefore, both these sites are larger in melanite A204 than in grossular (Z–O = 1.680 vs. 1.646 Å, Y–O = 2.004 vs. 1.937 Å, respectively). At the X site, Ca is joined by minor amounts of Na, Sr, LREE (larger) and of Mn, Mg, HREE (smaller), the average size of the X site is also larger than in grossular ($X1$–O = 2.366 vs. 2.328, $X2$–O = 2.515 vs. 2.488 Å, respectively), and also larger than expected on the basis of its population.

XAFS measurements at the commonly used REE L_{III} edge are impossible on this sample because of the presence of the Fe K_α interfering fluorescence line originating from the matrix, which cannot be resolved by a solid-state fluorescence detector. These problems can be overcome with the use of the Dy K-edge

because at these energies (> 53 keV) absorption edges and fluorescence lines do not overlap. We used the GILDA beamline at the European Synchrotron Radiation Facility (ESRF) in Grenoble, France, which offers a high photon flux in the hard X-ray range and a state-of-the-art 13-element hyper-pure Ge detector with fast digital electronics. The use of high energies in X-ray absorption spectroscopy is a rapidly developing field (Borowski et al. 1999; D'Acapito et al. 2002 and references therein), and can overcome various problems experienced when using the L-edges (Braglia et al. 1998, D'Acapito et al. 2001, Quartieri et al. 2002). It is especially useful when the simultaneous presence of atomic species with interfering edges and fluorescence lines prevents the recording of a good spectrum. and also allows data collection up to very high wave vectors. A limitation is the need for large amounts of material due to the low X-ray absorption cross-section at high energy. In order to access the very high energies required, we used the technique which exploits the third-order reflection of the beamline monochromator crystals (D'Acapito et al. 2002). The monochromator was operated in the dynamically sagittally focusing mode (Pascarelli et al. 1996). The data were recorded at 77 K, with a spacing of 0.7 eV in the XANES region and 2 eV in the extended part of the spectrum (EXAFS).

The raw fluorescence data are reported in Fig. 1, where the inset is an expanded view of the near edge region. Due to the short Dy core-hole lifetime, the lineshape in the vicinity of the absorption edge is strongly broadened, and hence no useful information could be obtained from the XANES region.

EXAFS oscillations were extracted from the raw data using the AUTOBK routine (Newville et al. 1993). Due to the extreme spectral broadening, care had to be taken to determine the correct absorption discontinuity (the edge jump), which might be incorrectly determined by standard approaches. In order to check the estimate of the edge jump (J) made with AUTOBK, we fitted the edge region with an arc-tangent function containing J (D'Acapito et al. 2002). In the case of the Dy_2O_3 standard, this procedure gave $J = 0.9$, in good agreement with the value of 1.0 determined by AUTOBK. The fitted value of the core-hole lifetime parameter was 21 eV, consistent with the theoretical value of 29 eV tabulated in FEFF8 (Ankudinov et al. 1998).

The raw, background-subtracted, spectra of the reference compound and the garnet sample are reported in Fig. 2a,b. Quantitative data analysis was limited to the first coordination shell of Dy. The FEFFIT (Newville et al. 1995) routine was used, with theoretical phase functions and amplitudes generated by FEFF8. Data analysis was performed in the ranges k 2.2÷11.0 $Å^{-1}$ and R 1.3÷2.0 Å, using a k-weight equal to 1.

The site preference of Dy in the garnet structure was deduced performing a number of simulations of the EXAFS signal of Dy in different coordination geometries (4 + 4, 6 + 2, 3 + 3). The best fit was obtained for the 4 + 4 model, which implies incorporation at the X site. The fit parameters were the Debye–Waller (DW) factor σ^2 and the Dy–O distances for the first two oxygen coordination shells. The reliability of the theoretical phases and amplitudes was successfully checked by applying them to the known structure of Dy_2O_3. The DW factors applied in the simulations of the garnet signal were set to 0.01 $Å^2$, similar to values determined previously for other REE in natural and synthetic garnets (Quartieri et al. 1999a, 2002).

Results and discussion

The Fourier transform (FT) of the Dy EXAFS signal from garnet A204 is shown in Fig. 3. The first peak (centred at about 1.8 Å) results from overlapping of the first two Dy–O coordination shells (i.e. those of the O atoms which built up the X site). The results of the Dy quantitative EXAFS analysis of this peak are reported in Table 1, where they are compared with the available data for REE occurring at the X site; the fit to experimental data is shown in Fig. 4.

Fig. 2a,b Background-subtracted EXAFS signals recorded at 77 K for Dy in the reference compound **a** and in the garnet sample **b**
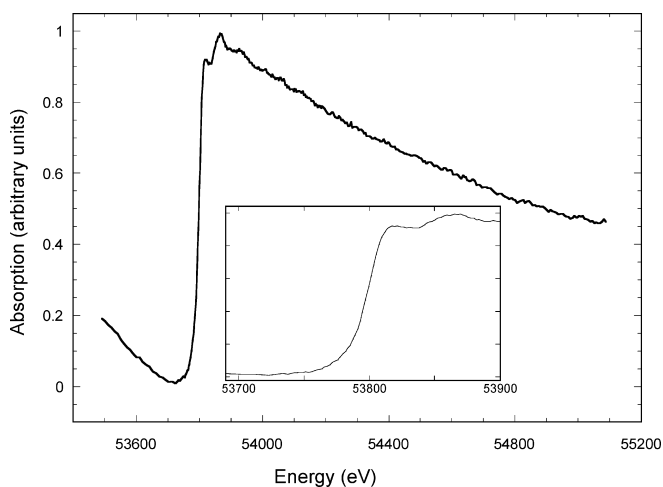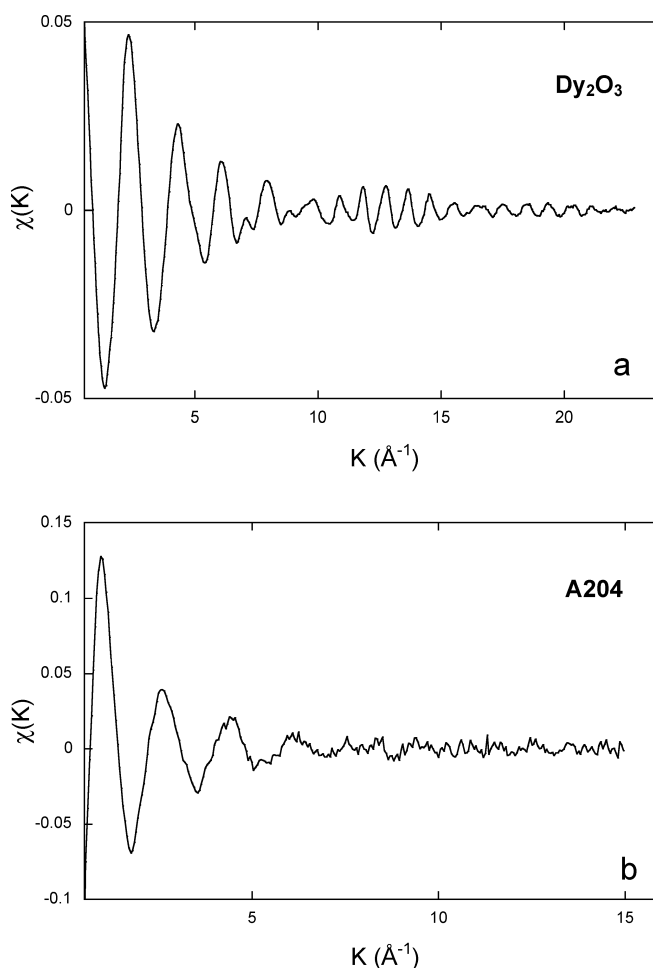

Fig. 1 Raw fluorescence data of Dy K-edge collected on the A204 melanite at 77 K. The *inset* is an expanded view of the near-edge region

A comparison may be attempted between the Dy–O values calculated in melanite A204 [$X1$–O = 2.31(1), $X2$–O = 2.41(3), $<X$–O$>$ = 2.36(2) Å] and those measured by single-crystal refinement of synthetic $Dy_3Fe_2Fe_3O_{12}$ ($X1$–O = 2.360, $X2$–O = 2.439, $<X$–O$>$ = 2.400 Å; Euler and Bruce 1965). As discussed in the introduction, the long-range geometry (i.e. that averaged over the studied crystal) of all the sites in the garnet structure, even of those whose composition does not vary, strongly depends on the overall composition. As a matter of fact, the X-site dimension reported for $Yb_3Al_2Al_3O_{12}$, $Yb_3Fe_2Fe_3O_{12}$, $Yb_3Ga_2Ga_3O_{12}$ by Euler and Bruce (1965) varies significantly with the size of the Y and Z cations (Table 1). In particular, the presence of larger Y and Z cations makes the Yb–O distances longer and the Yb coordination more regular [ΔX–O = ($X2$–O) $-(X1$–O) = 0.12, 0.114, 0.105, 0.082 Å, respectively, the changes in $X1$–O being much stronger than those in $X2$–O]. Also, the coordination geometry of Yb in Yb-doped grossular ($Ca_3Al_2Si_3O_{12}$) is different from that in $Yb_3Al_2Al_3O_{12}$ (the Yb–O distances are shorter, coherently with the presence of a smaller Z cation). In the same way, the Ca–O distances increases, and the Ca coordination becomes more regular, passing from grossular to melanite A204, where there is significant substitution of larger cations at both the Y and Z sites. As a consequence of this complex behaviour of the garnet structure, a reliable comparison can be done only for strictly similar overall compositions.

The work done in melanite A204 provides a unique opportunity to model the coordination geometry of trace REE and of Ca at the major-element level. Table 1 shows that the $X1$–O, $X2$–O and $<X$–O$>$ distances determined by XAFS analysis for the various REE are generally coherent with the changes in the ionic radii, as well as with the values independently estimated for Ca by single-crystal structure refinement, when the aggregate $<X$–O$>$ distance is corrected for the effects of the minor constituents (essentially Na, Mn and some Mg) based on the proper ionic radii (details are reported in Quartieri et al. 2002). More informative conclusions can, however, be drawn when comparing all the available data.

Figure 5 shows the $<X$–O$>$ distances for individual cations available in the literature. The large dimensional range of each cation in the different garnet compositions is clearly represented by the vertical piling of points relative to Yb, Dy and Ca. The corresponding changes in the regularity of the X polyhedron are reported in Table 1.

The most interesting feature is the change in the slope of the trends observed in each composition, although some of them are poorly constrained by the few available data. If the changes in geometry depended only on variations in the ionic radii, all the measured values should line up on or parallel to the dashed line, which is calculated by summing the radii of the cations to that of $^{[4]}O^{2-}$ (1.38 Å; Shannon 1976). On the contrary, the observed slopes are quite different, showing that the structural relaxation strongly depends on the overall composition. Using the XAFS data for Yb at 77 K and the structure refinement data of the relevant end members obtained at 100 K, we obtain that the slope is smaller, and thus the con-

Table 1 The available X–O distances and disorder parameters relevant for REE incorporation in garnets. Ionic radii in eight fold coordination. (Shannon 1976)

	i.r. (Å)	$X1$–O		$X2$–O		$<X$–O$>$ (Å)	ΔX–O (Å)
		R(Å)	σ^2 (Å^2)	R(Å)	σ^2 (Å^2)		
Melanite A204 at 77 K (a = 12.130 Å) (this work and Quartieri et al. 2002)							
Dy	1.03	2.31(1)	0.003	2.41(3)	0.005	2.36(2)	0.10
Nd	1.11	2.38(3)	0.002	2.47(3)	0.004	2.43(3)	0.09
Ce	1.14	2.39(4)	0.001	2.51(4)	0.004	2.45(4)	0.12
Ca[a]	1.12	2.374		2.523		2.449	0.149
Grossular (a = 11.848 Å) (sample 41 in Merli et al. 1995)							
Ca[a]	1.12	2.324		2.488		2.406	0.164
Yb-doped pyrope at 77 K (a = 11.462 Å) (Quartieri et al. 1999a)							
Yb	0.98	2.25(2)	0.005	2.33(2)	0.003	2.29(2)	0.08
Yb-doped grossular at 77 K (a = 11.850 Å) (Quartieri et al. 1999a)							
Yb	0.98	2.24(2)	0.008	2.38(2)	0.010	2.31(2)	0.14
$Yb_3Al_2Al_3O_{12}$ (a = 11.931 Å) (Euler and Bruce 1965)							
Yb[a]	0.98	2.283		2.397		2.340	0.114
$Yb_3Ga_2Ga_3O_{12}$ (a = 12.204 Å) (Euler and Bruce 1965)							
Yb[a]	0.98	2.302		2.407		2.355	0.105
$Yb_3Fe_2Fe_3O_{12}$ (a = 13.392 Å) (Euler and Bruce 1965)							
Yb[a]	0.98	2.335		2.417		2.376	0.082
$Dy_3Fe_2Fe_3O_{12}$ (a = 12.405 Å) (Euler and Bruce, 1965)							
Dy[a]	1.03	2.360		2.439		2.400	0.079

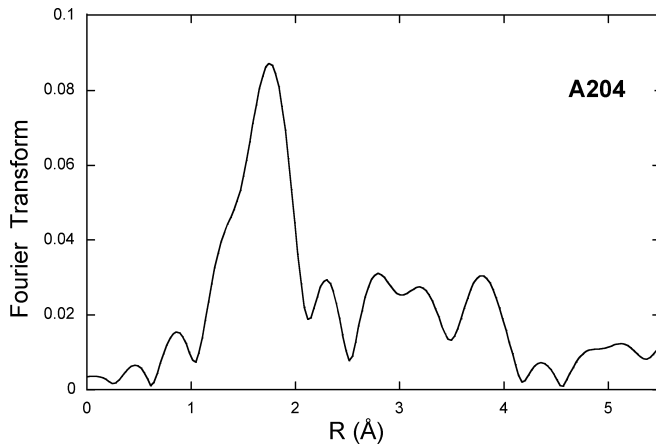[a] from single-crystal structure refinement

Fig. 3 Fourier transform of $k \chi(k)$ Dy signal in melanite A204
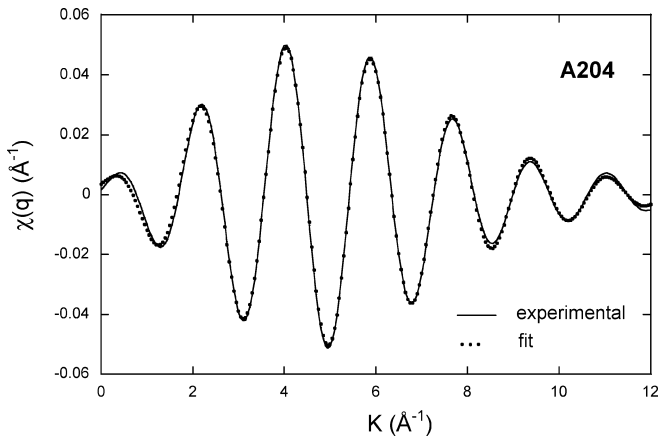

Fig. 4 Fit (*dotted line*) to the back Fourier transform (*full line*) of Dy K-edge data shown in Fig. 2 performed in the range 1.3–2.0 Å
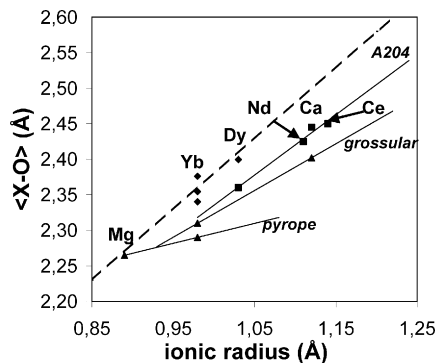

Fig. 5 Variations in the $<X–O>$ bond distances for different X-site cations in different garnet compositions. *Squares* this work and Quartieri et al. (2002); *diamonds* Euler and Bruce (1965); *triangles* Quartieri et al. (1999a). The *dashed line* is the theoretical dependence calculated by summing to the cationic radii that of $^{[4]}O^{2-}$ (1.38 Å)

straints against relaxation are stronger, in the more compact structure of pyrope (slope 0.2817) than in that of grossular (slope 0.6571).

Melanite A204 contains significant amounts of larger cations at both the Y and Z sites, which also allows a larger size of the X site (at room T, the $<Ca–O>$ distance is 2.406 in grossular and 2.449 in A204). We have corrected the $<Ca–O>$ value for T assuming the same thermal expansion as in grossular (Geiger and Armbruster 1997), and calculated a slope of 0.86, and an R^2 value of 0.98, larger than that of pyrope and grossular but still smaller than the ideal one. The high R^2 value of the linear regression validates the accuracy of high-energy XAFS analysis.

The observed deviations from the ideal slope indicate that a fully ionic bonding model is not adequate to model the garnet structure, especially for the compositions of petrologic relevance (e.g. the pyrope–grossular join).

The variation in the slopes implies that the X site has a different compliance for solid solution in the various garnet compositions; this compliance is related to the E_X value in terms of the elastic strain theory, and thus to the bulk modulus. Therefore, this conclusion is coherent with the decrease in the X-site bulk modulus with increasing grossular component observed by Van Westrenen et al. (2001) when applying the Blundy and Wood model to garnet-melt partition coefficients. However, this work provides a quantitative structural explanations for the observed variation, and also stresses the important role exerted by the composition of the Y and Z sites. Noteworthy, both approaches indicate a non-linear dependence on composition.

To sum up, XAFS investigations on REE behaviour in melanite A204 confirm that the elements examined all substitute after Ca at the X site. Also, comparison of the available data on natural and synthetic garnets, albeit obtained with different techniques, indicates that the local environment of a given element is strongly dependent on the overall garnet composition, i.e. on the population of all the structural sites. This result contrasts with the atomistic simulations done by Van Westrenen et al. (2003), who concluded that the local environments of the individual cations are relatively independent on major-element composition. Further work is therefore required to better understand this issue, which is rather crucial for modelling trace-element partitioning and thus for petrogenetic studies.

References

Ankudinov AL, Ravel B, Rehr JJ, Conradson SD (1998) Real-space multiple-scattering calculation and interpretation of X-ray-absorption near-edge structure. Phys Rev (B) 58: 7565–7576

Beattie P (1994) Systematics and energetics of trace-elements partitioning between olivine and silicate melts: implication for the nature of mineral/melt partitioning. Chem Geol 117:57–71

Blundy JD, Wood B (1994) Prediction of crystal-melt partition coefficients from elastic moduli. Nature 372: 452–454

Blundy JD, Wood B (2003) Partitioning of trace elements between crystals and melts. Earth Planet Sci Lett 210: 383–397

Borowski M, Bowron DT, DePanfilis S (1999) High-energy X-ray absorption spectroscopy at ESRF BM29, J Synchrotron Rad 6: 179–181

Bosenick A, Dove MT, Geiger CA (2000) Simulation studies on the pyrope–grossular garnet solid solution. Phys Chem Miner 27: 398–418

Braglia M, Dai G, Mosso S, Pascarelli S, Boscherini F, Lamberti C (1998) Pr K-edge X-ray absorption fine structure analysis of the local structure of Pr in fluorozirconated glasses. Appl Phys Lett 83:5065–5068

Calas G, Manceau A, Combes JM, Farges F (1990) Application of EXAFS in Mineralogy. In: Mottana A, Burragato F (eds) Absorption spectroscopy in mineralogy. Amsterdam, Elsevier pp 172–200

D'Acapito F, Mobilio S, Santos L, Almeida R (2001) Local environment of rare-earth dopants in silica-titania-alumina glasses: an extended X-ray absorption fine structure study at the K edges of Er and Yb. Appl Phys Lett 78: 2676–2678

D'Acapito F, Colonna S, Maurizio C, Mobilio S (2002) Multiple-order reflections from monochromating crystals for the collection of X-ray absorption spectra at extremely high energies. J Synchrotron Rad 9: 24–27

Euler F, Bruce JA (1965) Oxygen coordinates of compounds with garnet structure. Acta Crystallogr 19: 971–978

Geiger CA (1999) Thermodynamics of $(Fe^{2+}, Mn^{2+}, Mg, Ca)_3Al_2Si_3O_{12}$ garnet: a review and analysis. Mineral Petrol 66: 271–299

Geiger CA (2000) Volumes of mixing in aluminosilicate garnets: solid solution and strain behavior. Am Mineral 85: 893–897

Geiger CA, Armbruster Th (1997) $Mn_3Al_2Si_3O_{12}$ spessartine and $Ca_3Al_2Si_3O_{12}$ grossular garnet: structural dynamic and thermodynamic properties. Am Mineral 82: 740–747

Koninsberger DC, Prins R (eds) (1988) X-ray absorption. Wiley, New York

Lee PA, Citrin PH, Eisemberg P, Kincaid BM (1981) Extended X-ray absorption fine structure – its strengths and limitations as structural tool. Rev Mod Phys 53: 769–806

Merli M, Callegari A, Cannillo E, Caucia F, Leona M, Oberti R, Ungaretti L (1995) Crystal-chemical complexity in natural garnets: structural constraints on chemical variability. Eur J Mineral 7: 1239–1249

Newville M, Livins P, Yacoby Y, Rehr JJ, Stern EA (1993) Near-edge X-ray absorption fine structure of Pb: a comparison of theory and experiment. Phys Rev (B) 47: 14126–14131

Newville M, Ravel B, Haskel D, Rehr JJ, Stern EA, Yacoby Y (1995) Analysis of multiple-scattering XAFS using theoretical standards. Physica (B) 208–209: 154–156

Pascarelli S, Boscherini F, D'Acapito F, Hraty J, Meneghini C, Mobilio S (1996) X-ray optics of a dynamical sagittal focussing monochromator on the GILDA beamline at the ESRF. J Synchrotron Rad 3: 147–155

Quartieri S (2003) Synchrotron radiation in the Earth Sciences. In: Mobilio S, Vlaic G (eds.) Synchrotron radiation: fundamentals, methodologies and applications. Conference Proceedings vol. 82 Societá Italiana di Fiscìa, Bologna (Italy), pp 427–448

Quartieri S, Chaboy J, Merli M, Oberti R, Ungaretti L (1995) Local structural environment of calcium in garnets: a combined structure-refinement and XANES investigation. Phys Chem Miner 22: 159–169

Quartieri S, Antonioli G, Geiger CA, Artioli G, Lottici PP (1999a) XAFS characterization of the structural site of Yb in synthetic pyrope and grossular garnets. Phys Chem Miner 26: 251–256

Quartieri S, Chaboy J, Antonioli G, Geiger CA (1999b) XAFS characterization of the structural site of Yb in synthetic pyrope and grossular garnets. II: XANES full multiple scattering calculations at the Yb L_I- and L_{III}-edges. Phys Chem Miner 27: 88–94

Quartieri S, Boscherini F, Chaboy J, Dalconi MC, Oberti R, Zanetti A (2002) Characterization of trace Nd and Ce site preference and coordination in natural melanites: a combined X-ray diffraction and high-energy XAFS study. Phys Chem Miner 29: 495–502

Salters VJM, Longhi JE (1999) Trace element partitioning during initial stages of melting beneath ocean ridges. Earth Planet Sci Lett 166: 15–30

Shannon RD (1976) Revised effective ionic radii and systematic studies of interatomic distances in halides and chalcogenides. Acta Crystallogr (A) 32: 751–767

Ungaretti L, Leona M, Merli M, Oberti R (1995) Non-ideal solid-solution in garnet: crystal structure evidence and modelling. Eur J Mineral 7: 1299–1312

Van Westrenen W, Blundy JD, Wood BJ (1999) Crystal-chemical controls on trace element partitioning between garnet and anhydrous silicate melt. Am Mineral 84: 838–847

Van Westrenen W, Allan NL, Blundy JD, Purton JA, Wood BJ (2000) Atomic simulation of trace element incorporation into garnets — comparison with experimental garnet-melt partitioning data. Geochim Cosmochim Acta 64: 1629–1639

Van Westrenen W, Wood BJ, Blundy JD (2001) A predictive thermodynamic model of garnet-melt trace element partitioning. Contrib Mineral Petrol 142: 219–234

Van Westrenen W, Allan NL, Blundy JD, Lavrentiev Myu, Lucas BR, Purton JA (2003) Trace-element incorporation into pyrope-grossular solid solution: an atomistic simulation study. Phys Chem Miner 30: 217–229

Wood BJ, Blundy JD (1997) A predictive model for rare-earth-element partitioning between clinopyroxene and anhydrous silicate melt. Contrib Miner Petrol 129: 166–181

Wood BJ, Blundy JD (2002) The effect of H_2O on crystal-melt partitioning of trace elements. Geochim Cosmochim Acta 66: 3647–3656